ADVANCED MATERIALS INTERFACES
Open Access
www.advmatinterfaces.de

Ultra-Flexible μ-ECoG Arrays Based on PEDOT:PSS Micropillars

Alice Lunghi, Michele Bianchi,* Pierpaolo Greco, Riccardo Viaro, Michele Di Lauro, Luciano Fadiga, and Fabio Biscarini*

Devices capable of recording electrophysiological signals with high signal-to-noise ratio (SNR) and spatiotemporal resolution are crucial in neurological research. The introduction of flexible materials and conductive polymers in the fabrication of multi electrode arrays (MEAs) for electrocorticography (ECoG) enabled higher quality of recorded signals thanks to device conformability and to low-impedance electrodes. Advances in microfabrication techniques allow a dramatic reduction in electrode size, leading to highly-dense microelectrode arrays with increased spatial resolution. Here, the synergic contribution of surface micropatterning and of conductive polymers on the recording performance of a home-built μECoG device is explored. The device is fabricated through a combination of conventional and unconventional micropatterning techniques, leading to an ultra-conformable polydimethylsiloxane (PDMS) array featuring different-size flexible micropillars forests coated with a thin layer of poly(3,4-ethylenedioxythiophene) poly(styrenesulfonate) (PEDOT:PSS). The performance of the device is assessed in vitro by electrochemical impedance spectroscopy and in vivo by detecting somatosensory evoked potentials from the somatosensory cortex of a rat. The increasing of the geometric area has only limited effect on the recording capability in the in vivo model investigated. Nevertheless, the extremely high SNR values obtained place the proposed approach as an innovative and versatile strategy for the prototyping of ultra-conformable μECoG devices.

1. Introduction

Brain interfaces enabling the high-quality recording of neural signals from the surface of the cortex are highly desired for research and medical applications.[1–3] Microelectrocorticography (μECoG) recording commonly relies on high-density multi-electrode arrays (MEAs) put in direct contact with the brain surface.[4] For this reason, the meticulous optimization of the brain-device interface in terms of mechanical and electrochemical characteristics is mandatory to achieve suitable recording performances.[5,6] In the last decade, advances in material science and microfabrication technologies allowed the progressive miniaturization of the size and pitch of the electrodes introducing high-density microelectrodes array[7,8] and giving great impetus to research aimed at the design and the fabrication of innovative μECoG devices.[4,9,10] Mechanical compliance and low impedance are two of the essential characteristics contributing to the optimization of such devices. Mechanical compliance refers to the capability of the array to adapt to the curvilinear shape of the brain[2,7,11,12] and to avoid displacement caused by the micro-motion of the organ originated by vascular pulsation, fluctuation in respiratory pressure, and movements of the head.[13,14] By ensuring intimate contact with the brain, compliant μECoG MEAs demonstrated superior electrochemical coupling at the electrode-cortex interface, also outperforming traditional rigid platforms in terms of the quality of recorded signals.[7,15] To this end, polymeric materials likewise silicone-based elastomers, parylenes, and

A. Lunghi
Department of Physics
Mathematics and Informatics
Università di Modena and Reggio Emilia
Modena 41125, Italy
E-mail: alice.lunghi@unimore.it

The ORCID identification number(s) for the author(s) of this article can be found under https://doi.org/10.1002/admi.202500051

DOI: 10.1002/admi.202500051

A. Lunghi, M. Di Lauro, L. Fadiga, F. Biscarini
Centre for Translational Neurophysiology of Speech and Communication
Italian Institute of Technology
Ferrara 44121, Italy

M. Bianchi, F. Biscarini
Department of Life Sciences
University of Modena e Reggio Emilia
Modena 41125, Italy
E-mail: michele.bianchi@unimore.it

P. Greco, R. Viaro, L. Fadiga
Section of Physiology
Department of Neuroscience and Rehabilitation
University of Ferrara
Ferrara 44121, Italy

polyimides[15–17] represent an attractive alternative to silicon-based devices as they offer stiffness values orders of magnitude lower than metals, reducing the mechanical mismatch with the neural tissue.[18] In particular, silicones (e.g., polydimethylsiloxane, PDMS) exhibit the lowest Young's modulus (≈ 1 MPa,) excellent flexibility, and greater biocompatibility. For all these reasons PDMS has become widely used as the material of choice in epicortical recording.[19]

The recording of electrophysiological signals can be affected by different sources of noise that are introduced in the measures at various levels of the recording chain.[20] The overall noise originates from a complex integration of different types of noise, both biological likewise the spontaneous electrical activity of the brain,[21] and nonbiological such as flicker noise, thermal noise, electronic noise from the amplifier circuit, etc.[20,22,23] Thermal noise is introduced at the level of the electrodes and, since it depends on the random thermal motion of the charge carriers, its contribution is always present.[11,23] Although the importance of its contribution to the overall noise quantification is still controversial,[24–26] thermal noise remains the most addressable source of noise since it scales with impedance.[27] Therefore, the use of electroactive materials characterized by low intrinsic impedance is an accessible strategy to reduce the contribution of this form of noise, further contributing to the optimization of the recording interface.[22] A popular and effective strategy to achieve this goal is to coat microelectrodes with electroactive thin films[28] or, more effectively, with conductive polymers (CPs), and in particular with poly(3,4-ethylenedioxythiophene) polystyrene sulfonate (PEDOT:PSS).[2,7,15,29] Besides its intrinsic low impedance,[30] PEDOT:PSS owes its popularity in the field of neural recording to the mixed ionic-electronic conduction mechanism.[34,35] PEDOT:PSS, indeed, belongs to the subset of CPs called organic mixed ionic-electronic conductors (OMIECs), which thanks to their peculiar conduction mechanism are broadly used as signal transducing elements in bioelectronic devices that operate in aqueous electrolytes.[35,36] OMIECs are characterized by a conduction mechanism that couples electronic and ionic transport. In particular, the mixed conduction in PEDOT:PSS results from the presence of two distinct, yet intimately interpenetrated physical phases: the PEDOT domain that, thanks to the π-conjugated polymer chains account for electronic transport, and the PSS-rich phase, that accounts for ionic transport.[34,35] As such, PEDOT:PSS is capable of transducing ionic currents, typical of biological systems, into electronic ones, thus bridging the gap between the biotic and the abiotic components of the recording system.[36–38] Besides the conduction mechanism, the structural organization of PEDOT:PSS gives it a highly porous structure that is responsible for PEDOT:PSS high charge storage capacity and high charge injection limit.[39] Also, PEDOT:PSS porous structure allows for facile doping of the polymer to enhance its conductivity (up to 10^4 S cm^{-1}).[40,41] Other CPs like PANI and PPy have been employed in bioelectronics,[42] however, their use is strongly limited by important drawbacks. Both of them are difficult to dissolve in water, limiting access to traditional fabrication techniques such as electrodeposition and electrospinning and resulting in challenging and unsatisfactory processing.[43,44] Furthermore, PANI has a very poor conductivity in the physiological pH range[43] and PPy is extremely rigid and brittle,[45] making them not appropriate for interfacing with soft tissues. On the contrary, PEDOT:PSS can be easily processed in aqueous solutions and can be processed with traditional techniques; in particular PEDOT:PSS is extremely feasible for electrochemical polymerization, thus enabling optimal control of the coating.[46] Finally, PEDOT:PSS has demonstrated good biocompatibility toward neural cells,[33,47] thus becoming the workhorse material of bioelectronics applications.[29,36] Another fundamental aspect of μECoG recording is spatial resolution.[11] The introduction of high-density μMEAs opened the possibility to obtain high spatially resolved maps of the brain.[11] However, since impedance scales with electrode area,[48] the tendency to the miniaturization of the electrodes in favor of their density goes in the opposite direction to the need of lowering the impedance. In this scenario, an intriguing yet little explored strategy is offered by surface micropatterning.[49–51] Endowing microelectrodes surface with geometrically defined microstructures (i.e., micropillars) allows to increase microelectrodes surface area while preserving miniaturization[51,52] and spatial resolution.[51] In addition, tridimensional microstructures, such as nanowires, nanoneedles, mushroom-shaped microstructures and micropillars help create a biomimetic environment that can promote close interaction between cells and the microelectrodes surface.[41,53–57] Optimal entanglement of cells with surface microstructures reduces the effect of spatial averaging of the signal[56,58] and, especially in chronic implants, might contribute to limit signal extinction caused by glial scar formation.[59–61] However, most of these studies test this hypothesis only with cells cultured in vitro[55,56,58] while others are limited to electrochemical characterization of the micropatterned microelectrodes.[62]

In the last decade, research focused on engineering novel interfaces to record neural signals with high spatiotemporal resolution has flourished, leading to the development of sophisticated devices. For example, Khodagholy and colleagues[63] developed an highly-conformable μECoG array endowed with Au microelectrodes coated with PEDOT:PSS. The inherent lower impedance of PEDOT:PSS compared to Au led the PEDOT:PSS-coated microelectrodes to outperform the bare Au microelectrodes, while the extremely high density of the microelectrodes enabled an optimal spatial resolution.[7] The benefit of using PEDOT:PSS-coated microelectrodes instead of other conductive materials such as platinum and iridium oxide and combining the use of the CP with extreme conformability has been assed also by Vomero and co-workers,[15] that demonstrated the importance of mechanical compliant in preserving the reliability of the recorded traces over long term implantation. While the advantages of using PEDOT:PSS as active material, the importance of the substate's mechanical compliance and of the size and the density of the microelectrodes in achieving reliable and informative recordings have been widely demonstrated, very little has been done in terms of exploring the potential role of endowing the microelectrodes with hierarchically organized microstructures. A first attempt in this direction was made by Yang and Martin[49] who investigated how microporous PEDOT:PSS coating of the electrodes might influence the recording of neural signals, obtaining only a neglectable improvement. Later on, a similar study was published by Aqrawe and colleagues,[50] drawing a similar conclusion. An interesting work published in 2019[51] demonstrates how the presence of micropillars-like microstructures on the surface of Au microelectrodes resulted in higher values of SNR

compared to flat Au microelectrodes. The micropillars, in this case, were obtained by using lotus leaves as biotemplates. However, all these studies only consider irregular and not reproducible microstructures. We recently described the fabrication of flexible PDMS-based microelectrodes provided with PEDOT:PSS micropillars and the possibility to modulate relevant electrochemical properties, namely capacitance and electroactive surface area, by adjusting micropillars' diameter and areal density.[52] These electrodes showed great biocompatibility toward neural cells, also favoring a tight contact between the cells and the surface thanks to the presence of micropillars.[52] These electrodes join together all the requirements to optimize the performances of a μEcoG MEA as just described; hence, we envisioned their integration in an ultra-conformable μECoG MEA where the microelectrodes are patterned with PEDOT:PSS micropillars array on a thin and flexible PDMS substrate, with the aim to shed light on the length-scale dependence of epicortical neural recording. Notably, although highly regular micropillar arrays have been investigated for many different applications such as influencing and guiding neural growth and orientation,[64,65] recreating biomimetic environment[66,67] and electrophysiology,[68–70] their use in neural recording applications has not been reported in literature yet. In summary, the founding idea of the study is to investigate a strategy to reduce the impedance of the recording microelectrodes in order to obtain a better quality (i.e., higher signal-to-noise ratio, SNR) of the recorded signals. To obtain low impedance microelectrodes, we envisioned a straightforward strategy that couples the use of PEDOT:PSS with surface micropatterning. Indeed, PEDOT:PSS is characterized by intrinsic low impedance, while micropillars are expected to contribute to further reducing the impedance of microelectrodes by increasing microelectrodes' effective area (notably, impedance scales inversely with the area) while maintaining their lateral micrometer size and, consequently, spatial resolution. Impedance reduction is expected to correlate to neural signal recoding with a higher SNR, since noise, particularly thermal noise, is impedance dependent. Therefore, we devised two different micropillars geometries to provide a different increase in the geometric area of the microelectrodes and test our hypothesis. In addition, we decided to further lower the impedance by coating the microelectrodes with PEDOT:PSS and leveraging on a flexible substrate such as PDMS to ensure an optimal coupling between the electrodes and the brain surface. The effective decrease of impedance is predicted to be superlinear with the increase of geometrical area, as the capacitance of PEDOT:PSS electrodes is known to scale as the volume and not the area.[71,72] Here, we report the process that we specifically designed to fabricate such a device starting from scratch and demonstrate its capability to record somatosensory evoked potentials exhibiting outstanding values of signal-to-noise ratio.

2. Results and Discussion

2.1. Design of the "Neuropillar" Probe

The architecture of the Neuropillar array is detailed in **Figure** 1A(i). The device can be divided in three functional parts: contact pads at the right end, electrode tracks in the central stem, and the array of 16 microelectrodes at the left end. Aiming to study the effect of PEDOT:PSS micropillars on the recording performances, we designed Neuropillars so that half of the microelectrodes were endowed with micropillars (micropatterned electrodes), while the remaining eight were without micropillars (i.e., flat electrodes) (Figure 1A(ii)). To investigate the effect of different surface geometries, we devised two families of Neuropillar; one with micropatterned microelectrodes featuring micropillars with a nominal diameter of 4 μm (4μm_NP, (Figure 1B(i))) and the other one with micropillars showing a nominal diameter of 7 μm (7μm_NP, (Figure 1B(ii))). In both cases, the aspect ratio of the micropillars was fixed to 1 and the pitch, defined as the center-to-center distance between two adjacent pillars, was 15 μm. To comply with the constrain imposed by the fixed aspect/ratio, the height of micropillars must vary accordingly, hence micropillars with nominal diameters of 7 and 4 μm were designed to have a nominal height of 7 and 4 μm, respectively. Both micropatterned and flat microelectrodes are squares of 80 μm side and projected area of 6.4 10^3 μm^2 (Figure 1A(ii), zoom). Due to the presence of the micropillars, the geometric surface area of the single micropatterned electrode increases to ≈7.6 • 10^3 μm^2 (+ ≈20% vs flat electrode) for microelectrodes with 4 μm diameter micropillars and to ≈10.2 • 10^3 μm^2 (+ ≈60% vs flat electrode) for those with 7 μm diameter micropillars. The device is endowed with a grounding electrode composed of 16 interconnected electrodes (half of which are flat due to fabrication restrictions, (Figure 1A(ii))) that, in case of bipolar recording configuration, serves to record the physiological background activity from the local surroundings and to subtract it from the signal recorded by each microelectrode.[9] The device was designed with the view to record electrophysiological activity form the somatosensory barrel cortex of rats; thus, the whole sensing area including the reference electrode, covers an area of 2×2 mm^2 (Figure 1A(ii)).[73] During a recording session, it could happen that a micropatterned microelectrode is placed in correspondence of a neuron cluster that elicits high intensity signals, whereas a flat electrode records from a population that generates feebler waveforms. Since micropatterned electrodes are hypothesized to yield higher power of the recorded signals and a better signal-to-noise ratio (SNR) because of their major area compared to flat electrodes, such a recording scenario would unavoidably lead to biased recording outputs, not directly related to the geometry of the sensing electrode but rather to the nature of the "sensed" population of neurons.

To prevent such a possibility, we designed an equal distribution of the two microelectrode types (with micropillars and flat) in the shape of a checkerboard of four quadrants (Figure S1A, Supporting Information), populated two without micropillars and two with micropillars. Overall, we fabricated a device encompassing flat and micropillar microelectrodes on the same sensing area, thus taking down the chance of introducing recording biases as the one cited above. Furthermore, to investigate the effect of surface topography on the recording, we devised two distinct families of devices, namely 4μm_NP and 7μm_NP, that differ for the diameter of the micropillars (Figure 1B(i,ii)).

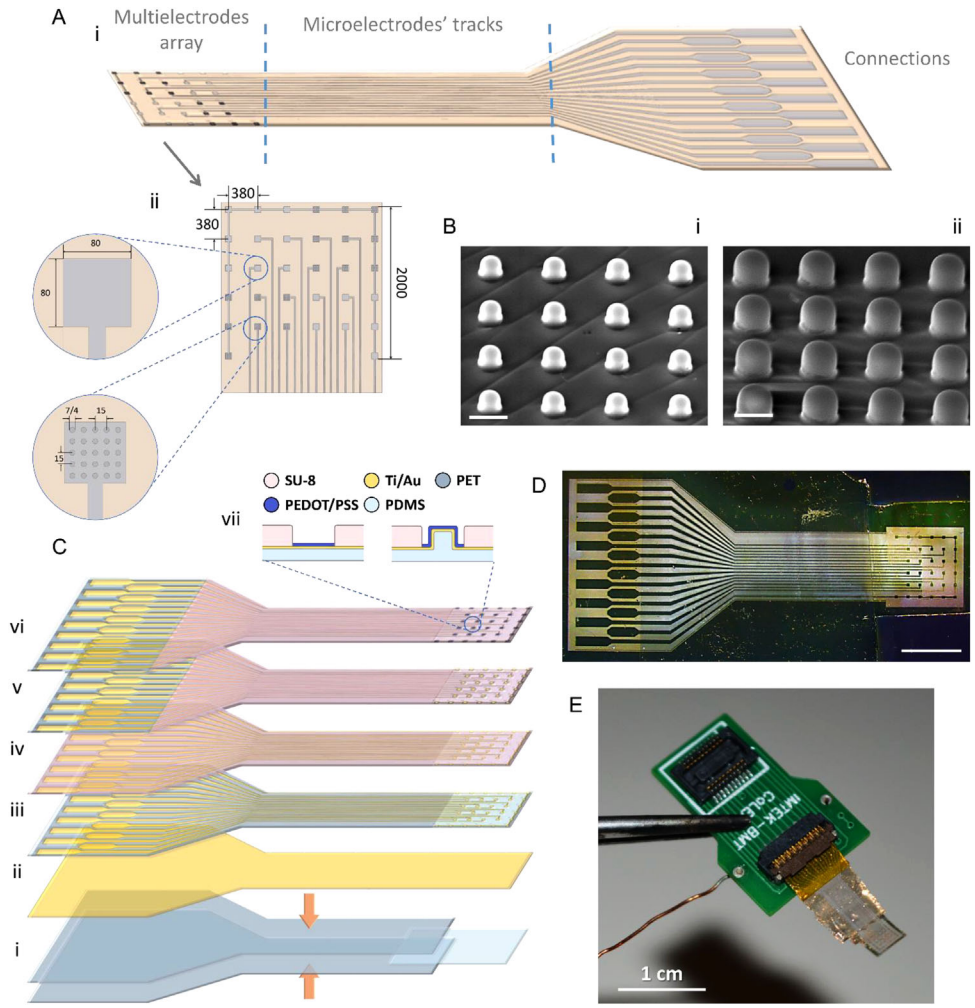

Figure 1. Design and fabrication of Neuropillar. A) Schematic representation of Neuropillar showing (i) the whole architecture of the device with the multielectrodes array (left), the central stem with microelectrodes' tracks and connections (right), and (ii) zoom of the multielectrodes array highlighting the arrangement of the 16 recording microelectrodes and of the ground electrode running around the perimeter of the array; distances are given in µm. B) Scanning electron micrographs of (i) 4 µm and (ii) 7 µm micropillars arrays; scale bar: 10 µm, magnification: 2500x. C) Neuropillar fabrication process. (i) The PDMS micropillars array (micropillars omitted) is encapsulated between two PET adhesive layers so that the micropillars array remains free standing; (ii) the surface of the PET/PDMS/PET sandwich is metalized with a thin layer of Ti and Au; (iii) the electrodes are obtained by removing the metal in excess by means of IR laser ablation; (iv) a protective layer of SU-8 is spin-coated on the device; (v) the SU-8 is selectively etched to expose only the recording sites and the connections (v); (vi) PEDOT:PSS is electrodeposited on each microelectrodes by means of chronocoulometry. (vii) Schematic representation of the final layered architecture of the microelectrodes. Not in scale. D) Optical micrograph of a 7um_NP µECoG MEA supported on a glass wafer after IR laser ablation (scale bar: 2 mm). The transparent area corresponds to the PDMS or to the PET layer (depending on the position considered) from which the gold was removed, while microelectrodes appear dark, shadowing the light source. E) The final aspect of a 7um_NP µECoG MEA snapped to the CaLEAF ZIF connector. From the picture, it is possible to guess the different mechanical properties of the central stem the connection pads (rigid) and the microelectrodes array (flexible).

2.2. Fabrication Procedure

An *ad hoc* multistep fabrication procedure was designed to obtain the Neuropillar array (Figure 1C(i-vi)). The most successful protocol we developed relies on a combination of different fabrication techniques, including soft-lithography (particularly replica molding),[74] metal sputtering, IR laser ablation, and electrochemical polymerization. Briefly, a PDMS micropillars array (thickness ≈80 µm), either with micropillars' diameter of 4 and 7 µm (aspect ratio of 1), was obtained by replica molding of silicon masters featuring micro-holes of the corresponding diameter (Figure S1B, Table S1, Supporting Information). The PDMS film was then encapsulated between two PET thin layers (≈7 µm) so that the area with micropillars array remained free-standing (Figure 1C(i)). In such a way, the flexibility and the mechanical properties of the PDMS micropillars array were not compromised and, at the same time, the central stem and the connections were stiff enough to both allow easy handling of the probe and ensure stable contact with the ZIF connector (see Experimental Section for further details). After metallization (Figure 1C(ii)); microelectrodes, tracks and contact pads were patterned by removing the metal in excess through high-precision IR laser

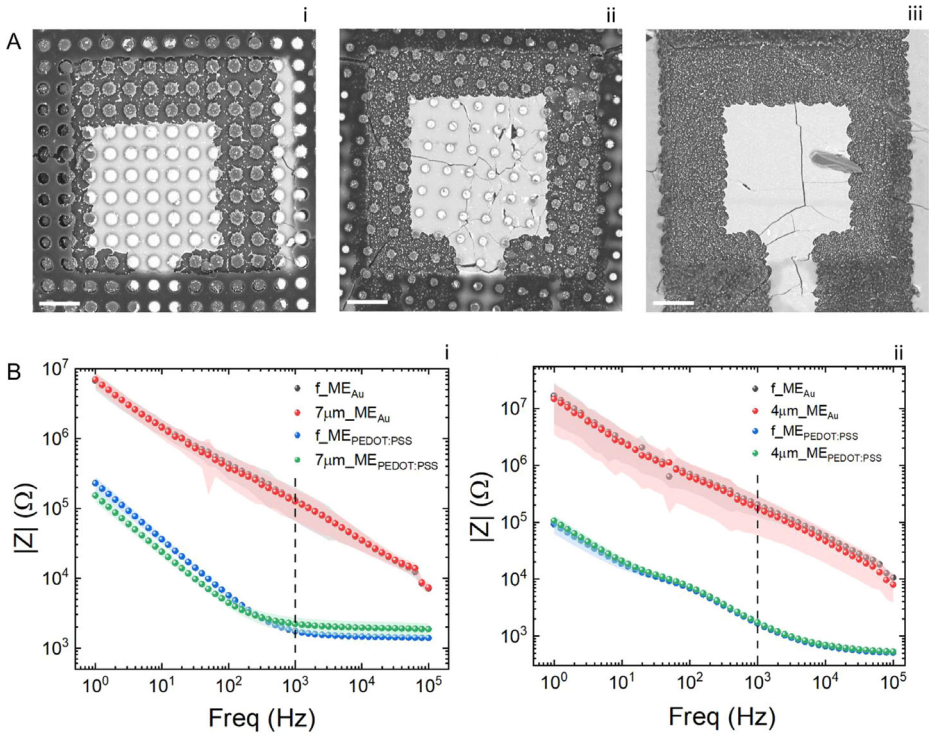

Figure 2. Morphological and electrochemical characterization of the microelectrodes. A) Representative SEM images of (i) 7μm_ME, (ii) 4μm_ME and (iii) f_ME; scale bar: 30 μm, magnification: 1000x. B) Bode plot showing EIS spectrum of the best performing (i) 7μm_NP and (ii) 4μm_NP device; dashed line is a guide-for-the-eye for $|Z|_{1kHz}$. EIS of 7μm_NP refers to the same device used for acute in vivo recording.

ablation (Figure 1C(iii)). A protective layer of SU-8 was added so that only the recording sites (microelectrodes) were exposed to the EDOT solution during the subsequent electrochemical polymerization process (Figure 1C(iv-vi)). The exploded layered architecture of the microelectrodes, either flat or endowed with micropillars, is shown in Figure 1C(vii). Figure 1D shows an optical view of the Neuropillar array after that connection (right), tracks, and microelectrodes (left) were patterned by means of IR laser ablation. Each recording channel (i.e., connection pad, electrode track, and microelectrode) is clearly identified and separated by the others, indicating that all the 16 electrodes are independent and insulated. The final appearance of the device, shaped into its final design and inserted into the CaLEAF ZIF connector, is shown in Figure 1E. The layered architecture of the device originates a step at the interface between the PDMS film and the upper PET layer; however, despite the step being taller than the thickness of the metallic layer (7 vs 30 nm) electrical conductivity was provided along the whole recording channel, as demonstrated by the electrochemical measurements reported hereafter (see "Electrochemical characterization"). Indeed, the sputtering process allows the deposition of Ti and Au in all directions of the space and not only perpendicular to the surface,[75] thus providing electrical connectivity at the PDMS/PET interface.

2.3. Characterization of the Microelectrodes and of the Neuropillar Array

Micropillar arrays obtained through PDMS replica (Figure 1B) accurately reproduced the characteristic dimensions of the master's microholes (Figure S1 and Table S1, Supporting Information). The average diameter and height of the micropillars were both ≈8.5 μm for the 7 μm array and ≈5 μm (diameter) and ≈4.8 μm (height) for the 4 μm array. **Figure** 2A(i–iii) shows the three types of PEDOT:PSS-coated microelectrodes investigated in this study: f_ME, 4 μm_ME and 7 μm_ME. The different materials making the layered structure of the microelectrodes (PDMS, Ti/Au, PEDOT:PSS) are characterized by distinguished mechanical behaviors. Clearly, PDMS is significantly softer and more flexible[76] than the Ti/Au and the PEDOT:PSS layers,[77] and these differences resulted in the formation of microcracks in the microelectrodes' conductive coating due to residual mechanical stresses.[78] Notably, as previously observed,[52] the presence of the micropillars reduces the number and the length of the microcracks compared to flat electrodes, confirming that the micropillars act as quenchers for the formation of microcracks. Moreover, as clearly visible in Figure 2A(i) and Figure S2 (Supporting Information), microcracks are almost absent in the 7μm_ME. The magnitude of the mechanical forces experienced by the electrodes is difficult to quantify. However, we speculate that the overall mechanical stress experienced by each device is comparable, thus we hypothesize that larger microstructures (i.e., 7 μm diameter micropillars) might be more capable to absorb mechanical stress than smaller ones (i.e., 4 μm diameter micropillars) (Figure 2A(ii) and Figure S3, Supporting Information). Nonetheless, the presence of fractures in the microelectrodes still allowed electrical conductivity of the microelectrodes as indicated by the Bode plots reported in Figure 2B.[52,78] Since the presence of the microcracks do not abruptly interrupt the physical continuum of the

PEDOT:PSS coating, the formation of percolative pathways is preserved and, consequently, so is the electrical conductivity. Overall, the presence of the micropillars contributes to the mechanical and structural stability of the microelectrodes, reducing the occurrence of pits and cracks, and preventing detrimental delamination of the different layers.

As mentioned in the introduction, mechanical compliance is a fundamental aspect of epicortical recording devices as a good coupling between the cortex and the microelectrodes accounts for the improved quality of the recorded signals.[2,7,10,15,63] Preliminary evaluation of the conformability of an epicortical recording device to the cortex is provided by assessing its capability to spontaneously wrap around a curved and wet surface.[79,80] According to the elastocapillarity model (see Supporting Information),[80] the spontaneous wrapping of a thin film around occurs when its bending stiffness (B) yields an elastocapillarity length (L_{EC}) smaller than the curvature radius (r) of the surface, represented by rat's barrel cortex ($r = 3$ mm).[15] Bending stiffness greatly depends on the thickness of the film; in our case, considering a thickness of the PDMS film of ≈80 µm, B is ≈ $4.3 \cdot 10^{-8}$ Nm, resulting in L_{EC} value ≈ 0.84 • mm (see Table S2, Supporting Information). Hence, according to this model, the PDMS film used as a substrate accounts for the great conformability of the device.

2.4. Electrochemical Characterization

Bode plots reported in Figure 2B(i,ii) show the impedance spectrum of representative 7µm_NP and 4µm_NP prior and after coating the microelectrodes with PEDOT:PSS. During the electrodeposition process, the charge was limited to 250 mC cm^{-2}, resulting in an estimated PEDOT:PSS thickness of ≈165 nm. This value was obtained based on preliminary experiments aimed at determining the thickness of PEDOT:PSS layers resulting from the deposition of different charge densities on flat gold-coated PDMS. Furthermore, for lower values of charge density (e.g., 125 mC cm^{-2}) it was difficult to appreciate the contribution of the PEDOT:PSS coating to the impedance of the microelectrodes, while for higher values (e.g., 500 mC cm^{-2}) the thickness of conducting polymer layer was such that it deformed the desired aspect ratio of the micropillars. The electrochemical impedance of the microelectrodes plays a pivotal role in the quality of the recorded signals since it scales with thermal noise;[22] thus, electroactive coating capable of reducing impedance modulus (|Z|) of the microelectrodes is highly desired as they can lead to higher signal-to-noise-ratio in vivo.[15,81] Electrodeposition of the conductive polymer resulted in a bold decrease of |Z| across the investigated frequency spectrum; being this the typical behavior of metallic electrodes when coated with PEDOT:PSS.[30] Regardless of the surface microstructure, EIS spectrum of PEDOT:PSS-coated microelectrodes is smoother than their metallic counterparts: during the electrodeposition process, PEDOT:PSS conceals the microcracks of the gold layer and forms new percolation paths providing better electrical conductivity.[52] The impedance spectrum of 4µm_NP and 7µm_NP appear quite different. One of the main reasons of such difference can be found in the presence of more and longer microcracks in 4µm_MEs than in 7µm_MEs: the higher the number of microfractures and the longer their extension, the more hindered the formation of percolative pathways, thus resulting in the better impedance spectrum of the 7µm_NPs. In the frequency band between 100 Hz and 1 kHz of 4µm_NP there is a bump that can be ascribed to a non-optimal charge transfer between the conductive polymer and the underlying Au layer, likely due to the presence of the microcracks spotted in the SEM images.[71] Commonly, impedance characterization of neural recording microelectrodes is limited to the investigation of impedance values at the frequency of 1 kHz ($|Z|_{1\ kHz}$). As the main information content in action potential is conserved around this frequency, $|Z|_{1\ kHz}$ is generally taken as a comparative measure.[82] Both for 4µm_NP and 7µm_NP, the electrodeposition of PEDOT:PSS decreased the value of $|Z|_{1\ kHz}$ by two orders of magnitude, dropping from ≈2×10^5 Ω (gold microelectrodes) to ≈2×10^3 Ω (PEDOT:PSS microelectrodes), either for flat and micropillars microelectrodes. Such values of $|Z|_{1\ kHz}$ are in good agreement with what reported in literature for similar PEDOT:PSS-based microelectrodes.[29] However, since relevant information are not limited to the frequency of 1 kHz, but rather spread over a broader frequency spectrum, the value of the cutoff frequency (i.e., the frequency encompassing the shift between the resistive behavior – high frequencies – and the capacitive behavior – low frequencies) represents an appealing alternative to $|Z|_{1kHz.}$[22] Interestingly, the value of the cutoff frequency is very different between the two µECoG MEAs. Cutoff frequency of 4µm_NP is ≈$2 \cdot 10^3$ Hz either considering flat or micropillars microelectrodes. 7µm_NP exhibits different cutoff frequencies of flat microelectrodes (≈500 Hz) and micropillars microelectrodes (≈250 Hz). Broadening of the frequency-independent region should accounts for lower level of thermal noise during the recording as |Z| remains low in a wider area of the spectrum.[71] The overall impedance trend of 4µm_NP, however, suggests the presence of a resistive component dependent on the electrolyte, raising concerns about the occurrence of pinholes in the protective layer. This phenomenon is likely related to the reduced mechanical stability toward microcracks conferred by 4-µm micropillars compared with 7-µm micropillars and led us to exclude 4µm_NP from in vivo recording experiments. To be highlighted, EIS also indirectly provides an important clue about the effective insulation of the recording channels (i.e., absence of crosstalk among close tracks). Indeed, impedance spectrum for each microelectrode of all the devices before and after PEDOT:PSS electrodeposition were comparable in terms of |Z| magnitude and overall trend, although not well overlapped (Figure S4, Supporting Information), suggesting independent signal recording from each channels.

2.5. In Vivo Validation of the Neuropillar Array

Acute recording of somatosensory evoked potentials (SEPs) was selected as recording mode to achieve the proof-of-concept of the capability of the Neuropillar arrays to properly record electrophysiological signals from the rat cortex (**Figure 3A**). SEPs represent an excellent target for the validation of recording devices since their characteristic waveform and high-intensity (hundreds of µV) have been extensively characterized (e.g., number of peaks, onset time after trigger, amplitude, etc.).[83] In addition, SEPs can be easily triggered by stimulating the whiskers of the animal. Given the better in vitro electrochemical performance

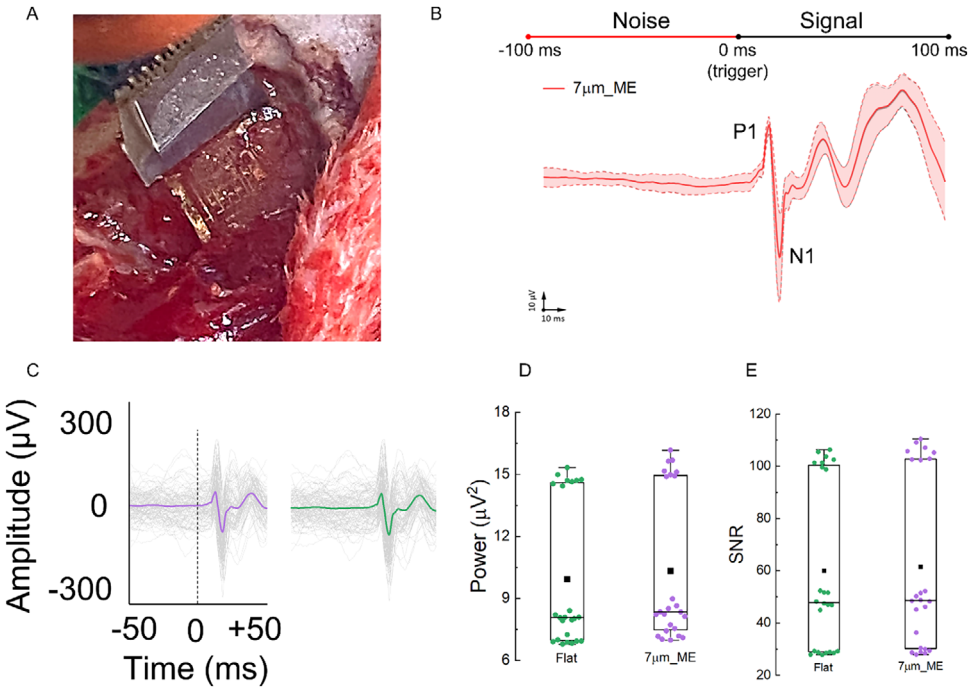

Figure 3. In vivo recording of SEPs using a 7µm_NP. A) Picture of the 7µm_NP array placed on the somatosensory cortex of the rat during the acute recording. B) SEP waveform (red solid line) obtained by averaging SEPs recorded by all micropatterned electrodes of the 7µm_NP array during an acute recording. All SEPs are time locked at the moment of the trigger, marked as 0 ms; spontaneous activity recorded in the 100 ms before the trigger is defined as noise, and elicited activity recorded in the 100 ms after the trigger is defined as a signal. C) Typical response of a 7µm_NP array showing characteristic SEP waveforms recorded by microstructured (purple) and flat (green) microelectrodes. The trigger is marked at 0 ms; SEP (colored line) is obtained by overlapping 100 trials (gray) for each microelectrode. D) Power of the signal of flat (green) and microstructured (purple) microelectrodes; E) SNR values of flat (green) and microstructured (purple) microelectrodes. In D and E data points refer to three acute recording sessions performed with the same device placed over three different positions of the somatosensory cortex (24 data points for each microelectrode category).

and mechanical stability, we opted to test in vivo only 7µm_NP and not 4µm_NP. Furthermore, we had previously demonstrated that microelectrodes endowed with micropillars of 7 µm diameter provide better modulation of electrochemical properties (i.e., capacitance and electroactive surface area).[52] Even though we considered an in-probe ground electrode, we opted for unipolar recording (i.e., using a screw implanted in the skull as grounding) because the in-probe ground might record some signal of interest and, since electrical activity collected by the ground electrode is subtracted to the recordings of the microelectrodes, bipolar recording could lead to the loss of some information.[9] The presence of SEP's characteristic hallmarks, namely the first positive peak (P1) and of the first negative peak (N1)[73] at the correct latency time with respect to the trigger (P1 after ≈13 ms; N1 after ≈17 ms; Figure 3B) confirmed the nature of the recorded signals. Figure 3C shows the typical response of microstructured and flat microelectrodes of the Neuropillar array; notably all the 16 recording channels could detect and record SEPs waveforms.

To quantitively explore the contribution of micropatterning on the recording output, we characterized flat and micropillar microelectrodes by means of two features: power and SNR.[15,84,85] Noise and signal were defined as the electrical activity 100 ms before and 100 ms after the trigger (Figure 3B), respectively. Either for flat or micropillar microelectrodes, the average power of the noise (Pwr_N) was close to zero (0.19 ± 0.07 μV^2), accounting for the little information content associated to spontaneous activity. The average power of the signal (Prw_S) was similar between the two types of microelectrodes (9.9 ± 3.5 μV^2 for flat microelectrodes and 10.3 ± 3.6 μV^2 for micropatterned microelectrodes) and in both cases was significantly higher than Pwr_N (p-value < 0.01). Pwr_S values of micropillar microelectrodes can be clustered in three different groups (Figure 3D), with each cluster corresponding to one acute recording session. Notably, the same clustering could not be appreciated for Pwr_N. Since we defined SNR as Pwr_S/Pwr_N, the difference between the average SNR of flat microelectrodes and micropillar microelectrodes was negligible and the clustering of SNR values was comparable with that of Pwr_S (Figure 3E). It is worth noticing that, because of the one-order-of-magnitude difference between Pwr_S and Pwr_N, the average SNR values of flat (60 ± 32) and micropatterned (62 ± 33) microelectrodes resulted considerably high.[4,29] The comparable behavior of the microelectrodes suggests that, despite dramatically increasing microelectrodes' surface area (+ 60% for 7µm_ME with respect to f_ME), surface micropatterning has only limited effects in terms of recording performances. Similar results on the effect of surface morphology were reported by Aqrawe and colleagues[50] when comparing recording outputs of flat and macroporous PEDOT:PSS electrodes. Therefore, we ascribe the high values of SNR to the combined effect of mechanical compliance and low impedance achieved by the use of ultraflexible PDMS as substrate and of PEDOT:PSS as electroactive material. However, the presence of micropillars positively affects

the stability of the microelectrodes. At the end of the recording experiments, EIS spectrum of flat and micropillars electrodes was shifted to higher impedance values (Figure S5A, Supporting Information), but while $|Z|_{1\ kHz}$ of flat microelectrodes increased of two orders of magnitude, $|Z|_{1\ kHz}$ of micropillars microelectrodes increase of just one order of magnitude. This behavior is in line with the major delamination of the PEDOT:PSS coating experienced by flat microelectrodes (Figure S5B, Supporting Information), confirming that micropillars contribute to the stability of the conductive coating.

3. Conclusion

In this work, we successfully demonstrated the fabrication of an ultra-flexible μECoG device obtained starting from scratch and by designing an ad hoc fabrication procedure. Since mechanical compliance and low impedance are the two characteristics of a μECoG that impact the most on the quality of the recording output, we combined several techniques to assemble a μMEAs based on a PEDOT:PSS-coated PDMS micropillars array. We reported, for the first time, the introduction of highly regular micropillar arrays in the field of epicortical neural recording, investigating their role as key elements to increase the area of the microelectrodes to further lower the impedance of the latter, also combining the use of the conductive polymer. The recording capability of the device was validated by recording SEPs from the somatosensory cortex of a rat. Neuropillar precisely detected the waveforms with high values of power and signal-to-noise ratio, even though it was not possible to observe differences between recording outputs of flat and micropillar microelectrodes. However, SEPs are high-intensity signals, thus the contribution of noise on the recording is less impacting than for single spikes. Further experiments aimed at recording such signals will provide more insights into the role of micropillars in epicortical recording. Finally, we introduced the possibility of precisely controlling the surface area and the tridimensional structure of soft microelectrodes, adding a further level of dimensional control. The use of soft lithography as a tool for integrating defined structures on the surface of microelectrodes paves the way for finer tuning of microelectrode geometrical features than standard photolithography and wet patterning techniques (e.g., electrochemical deposition, spin coating, wet etching, etc.). The results obtained so far suggest that other patterning geometries and microstructures are worth testing to elucidate the role of micropatterning in epicortical recording.

4. Experimental Section

Fabrication of the Device: Microholed silicon (Si) masters were fabricated by reactive ion etching as previously described.[52] PDMS micropillar arrays were obtained by replica molding method using Sylgard 184 elastomer kit (Dow Europe GmbH, Horgen, Switzerland). The silicone elastomers base and the curing agent were mixed in a 10:1 v/v ratio; the mixture was degassed in a vacuum, then a volume of 1.5 mL was poured onto the Si master and spin coated using a two-step protocol (first step: 20 sec, 100 rpm, 500 rpm min^{-1}; second step: 45 sec, 1000 rpm, 500 rpm min^{-1}). The first step allowed the mixture to penetrate intro the microholes and the second one to remove the mixture in excess. After curing overnight at 60 °C, the PDMS film was gently removed by the master and fixed onto an adhesive layer of polyethylene terephthalate (PET) paying attention to have the micropillars oriented upward and to leave the area of the array free standing. The PET adhesive layer was previously fixed (adhesive side up) on a microscope glass slide employed as support. A 7 μm-thin layer of PET was used to encapsulate the PDMS on the adhesive layer. The PET/PDMS/PET sandwich was sputtered with a thin layer of Ti (≈3 nm, time: 1 min, average current: 30 mA) and, subsequently, with a layer of gold (≈30 nm, time: 3 min, average current: 18 mA) using a Q150RS DC magnetron sputter (Quorum Tech, London, United Kingdom) operating in argon rarefied atmosphere (≈ 10^{-1} mbar). Electrodes, tracks, and contact pads were obtained by removing the metal in excess by means of infrared laser ablation (1064 nm, 0.1 mW) with built-in-house equipment. It was worth noting that the resulting microelectrodes were independent of each other since by removing the metal in excess each of them was insulated from the neighbors, and results were individually addressable (as described later in this paragraph). At this point, a 2 μm-thick SU-8 (Kayaku Advanced Materials, MA, USA) layer was spin coated on the stack and soft baked (1 min, 95 °C) with a thermal ramp to preserve the gold film. The device was then aligned with a shadow mask designed to shade the microelectrodes and the contact pads using a MjB4 mask aligner (Suss Microte, Garnich bei Munchen, Germany) and exposed to UV light (356 nm) to allow the cross-linking of the exposed photoresist. After development, the device was trimmed in its final form using a surgical blade, removed from the support glass slide, snapped to the CaLEAF zero-insertion-force (ZIF) connector (IMTEK-BKT, Freiburg, Germany), and connected to the ZIF-clip Analogic Headstage (Tucker-Davis Technologies, FL, USA). The latter terminates with a printed circuit board (PCB) that features 17 pins, each of which corresponds to one of the microelectrodes of the array (16 recording channels plus 1 ground reference electrode), allowing each to be contacted individually at a time. To precisely control the amount of the deposited charge and of the corresponding thickness of the PEDOT:PSS layer, electrodeposition was carried out by means of chronocoulometry. The charge was limited to 250 mC cm^{-2}, using a large area platinum mesh (15×15 mm^2) as a counter electrode (CE) and a standard $Hg|Hg_2Cl_2$ electrode as a reference electrode (RE). The microelectrodes of the array were used as working electrodes (WE) one at a time by contacting the corresponding pin on the PCB. The electrochemical cell was filled with a solution of 0.01 M ethylenedioxythiophene (EDOT, Sigma–Aldrich, MO, USA) and 0.8% w/w poly(sodium 4-stryrenesulfonate) (NaPSS, Sigma Aldrich, MO, USA) in MilliQ water and the potentiostat (Gamry Reference 600, Gamry Instruments, PA, USA) was set to supply a constant potential (0.9 V) to the WE.

Device Characterization: Scanning electron microscopy (SEM) images of the microelectrodes and of the Neuropillar array were acquired using a SEM XPV Zeiss EVO 40 (Carl Zeiss, Germany) operating in high vacuum and electron high tension (EHT) of 15 kV. Before imaging, samples were mounted on metal stubs and sputtered with a 10 nm layer of gold using a Q150RS DC magnetron sputter (Quorum Tech, London, United Kingdom). The electrochemical properties of the microelectrodes were measured by means of electrochemical impedance spectroscopy (EIS). EIS of gold and PEDOT:PSS-coated microelectrodes was measured in the frequency range 1–10^5 Hz using a three electrodes electrochemical cell filled with a physiological solution (NaCl, 0.15 M). An Ag|AgCl (3 M KCl) was used as RE and a large area platinum mesh (15×15 mm^2) as CE. Neuropillar array was immersed in the saline solution; each electrode was individually contacted as described above and used as WE.

The thickness of the PEDOT:PSS layer was investigated by means of atomic force microscopy (AFM) using a Park XE7 AFM system (Park System, Suwon, Republic of Korea). AFM was operated in tapping mode, in air and at room temperature, using a premounted silicon cantilever with Al backside reflective coating, typical curvature radius ≈7 nm, elastic constant ≈26 N m^{-1}, and resonance frequency ≈300 Hz (OMCL-AC160TS, Olympus Micro Cantilever, Tokyo, Japan). To obtain this value, defined amount of charge densities ranging from 125 to 500 mC cm^{-2} with intervals of 25 mC cm^{-2} were electrodeposited on flat surfaces of gold-metallized PDMS using the same electrodeposition setup that was employed for the fabrication of μECoG devices. The Au-coated PDMS sheets were contacted with silver conductive paste and used as WE. A scratch was then obtained in the PEDOT:PSS layer and the AFM was used to measure

the height of the step, corresponding to the thickness of the conductive layer.

In Vivo Validation: Animal experiments were designed in compliance with the guidelines established by the European Communities Council (Directive 2010/63/EU, Italian Legislative Decree n. 26, 4/3/2014), and the protocol was approved by the institutional review board of the University of Ferrara and the Italian Ministry of Health (permission n. 989/2020-PR). An adult Wistar rat (≈400 g) was used as an animal model. At this stage of the project, the aim was to verify the capability of our newly developed array to record electrophysiological signals, the reason for which it was opted for the use of just one animal to accomplish the 3Rs principle and avoid further sacrifice of animals. On the day of the experiment, the animal was anesthetized with an intraperitoneal injection of a mixture of 30 mg k^{-1}g of tiletamine/zolazepam hydrochloride (Zoletil) and 5 mg k^{-1}g xylazine hydrochloride (Rompun). Anesthesia was maintained upon the whole duration of the experiment with additional administration of anesthetic (typically every 30–40 min); the level of anaesthetization was periodically monitored by testing the absence of hind limb withdrawal reflex. To expose the left somatosensory cortex, the anesthetized animal was placed on a stereotaxic apparatus to avoid movements of the head. After trimming head hairs, the skin was incised for a total length of 2 cm following the midline of the cranium, and the skull was exposed by retracting muscle and connective tissue. A 5×5 mm^2 craniotomy in the parietal bone was executed to expose the somatosensory cortex. During the entire surgical process, the operated area was maintained clear and hydrated by dispensing sterile saline solution. The animal was then placed in a faradic cage to reduce electromagnetic interference from the environment and the µECoG MEA was placed on the exposed area of the somatosensory cortex. Neural traces were collected using a Tucker Davis Technologies multi-channel recording system 3 (Tucker Davis Technologies, FL, USA) that was connected with the array via intermediate supplies. Briefly, starting from the brain side, the device was first snapped in the CaLEAF ZIF (IMTEK, Freiburg, Germany) that was then connected to the ZIF-Clip Analogic Headstage (Tucker Davis Technologies, FL, USA). The ZIF-Clip, in turn, was connected to a PZ2-256 battery-powered pre-amplifier (Tucker Davis Technologies, FL, USA) and to the R2Z real-time processor (Tucker Davis Technologies, FL, USA). SEPs were elicited by deflecting the whiskers of the animal (i.e., right whiskers, contralateral to the exposed somatosensory cortex) using an in-house built system endowed with a brush allowed to move only along the horizontal plane. The stimulation protocol consisted of a sine waveform of 12 ms and amplitude of 500 µm (matching the displacement of the whiskers brush) that was repeated 100 times with 4 s pause between each repetition so that the total time of a recording block was ≈6 min. At least three recording blocks were acquired on the same number of different positions on the exposed somatosensory barrel cortex. to acquire a significant set of independent data without sacrificing additional animals.

During the acquisition, data were band-pass filtered from 300 to 6000 Hz to remove environmental noise. To obtain the typical SEP waveform, the 100 trials recorded were averaged point-by-point for each electrode. Power spectrum density (PDS) was computed for intervals of 100 ms before and after the trigger (Hamming windowing function, windows overlap 50%) and integrated over the 3–300 Hz frequency band (local field potential, LFP) to obtain the power of the noise (before the trigger) and the signal (after the trigger). The signal-to-noise ratio was calculated as the ratio between the power of the noise and the power of the signal. Data were computed using OriginPro 2020 (OriginLab Corporation, MA, USA).

Supporting Information

Supporting Information is available from the Wiley Online Library or from the author.

Acknowledgements

The authors are grateful to Dr. Andrea Toma (Clean Room Facility, Italian Institute of Technology, Genova, Italy) for the kind supply of the microholed silicon masters. The manuscript was revised and approved by all the authors; the final version has been approved by all authors.

Conflict of Interest

The authors declare no conflict of interest.

Data Availability Statement

The data that support the findings of this study are available from the corresponding author upon reasonable request.

Keywords

conductive polymers, electrodeposition, epicortical recording, microfabrication, PDMS, somatosensory evoked potential

Received: January 17, 2025
Revised: February 26, 2025
Published online: March 20, 2025

[1] N. J. Hill, D. Gupta, P. Brunner, A. Gunduz, M. A. Adamo, A. Ritaccio, G. Schalk, *JoVE* **2012**, *64*, 3993.
[2] E. Delfino, A. Pastore, E. Zucchini, M. F. P. Cruz, T. Ius, M. Vomero, A. D'Ausilio, A. Casile, M. Skrap, T. Stieglitz, L. Fadiga, *Int. J. Neur. Syst.* **2021**, *31*, 2150025.
[3] S. Kellis, L. Sorensen, F. Darvas, C. Sayres, K. O'Neill, R. B. Brown, P. House, J. Ojemann, B. Greger, *Clinical Neurophysiology* **2016**, *127*, 591.
[4] M. Vomero, E. Castagnola, F. Ciarpella, E. Maggiolini, N. Goshi, E. Zucchini, S. Carli, L. Fadiga, S. Kassegne, D. Ricci, *Sci. Rep.* **2017**, *7*, 40332.
[5] M. Shokoueinejad, D.-W. Park, Y. Jung, S. Brodnick, J. Novello, A. Dingle, K. Swanson, D.-H. Baek, A. Suminski, W. Lake, Z. Ma, J. Williams, *Micromachines* **2019**, *10*, 62.
[6] L. Yao, Y. Qin, X. Li, Q. Xue, F. Liu, T. Cheng, G. Li, X. Zhang, W. Lai, *InfoMat* **2023**, *5*, e12410.
[7] D. Khodagholy, J. N. Gelinas, T. Thesen, W. Doyle, O. Devinsky, G. G. Malliaras, G. Buzsáki, *Nat. Neurosci.* **2015**, *18*, 310.
[8] C. Henle, M. Schuettler, J. Rickert, T. Stieglitz, in *Towards Practical Brain-Computer Interfaces*, (Eds.: B. Z. Allison, S. Dunne, R. Leeb, J. Del R Millán, A. Nijholt), Springer, Berlin, Heidelberg **2012**, pp. 85–103.
[9] K. A. Ludwig, R. M. Miriani, N. B. Langhals, M. D. Joseph, D. J. Anderson, D. R. Kipke, *Journal of Neurophysiology* **2009**, *101*, 1679.
[10] D. Khodagholy, J. N. Gelinas, Z. Zhao, M. Yeh, M. Long, J. D. Greenlee, W. Doyle, O. Devinsky, G. Buzsáki, *Sci. Adv.* **2016**, *2*, 1601027.
[11] M. E. J. Obien, K. Deligkaris, T. Bullmann, D. J. Bakkum, U. Frey, *Front. Neurosci.* **2015**, *8*, https://doi.org/10.3389/fnins.2014.00423.
[12] G. Li, Y. Gong, S. Fang, T. You, R. Shao, L. Yao, C. Liu, C. Wu, J. Niu, W.-Y. Lai, *Sci. China Mater.* **2024**, *67*, 1481.
[13] A. Gilletti, J. Muthuswamy, *J. Neural Eng.* **2006**, *3*, 189.
[14] M. S. Fee, *Neuron* **2000**, *27*, 461.
[15] M. Vomero, M. F. Porto Cruz, E. Zucchini, F. Ciarpella, E. Delfino, S. Carli, C. Boehler, M. Asplund, D. Ricci, L. Fadiga, T. Stieglitz, *Biomaterials* **2020**, *255*, 120178.
[16] A. Victor, J. Ribeiro, F. S. Araujo, *Journal of Mechanical Engineering and Biomechanics* **2019**, *4*, 1.

[17] I. Miranda, A. Souza, P. Sousa, J. Ribeiro, E. M. S. Castanheira, R. Lima, G. Minas, *JFB* **2021**, *13*, 2.
[18] A. Mata, A. J. Fleischman, S. Roy, *Biomed. Microdevices* **2005**, *7*, 281.
[19] J. Voros, G. Courtine, A. Larmagnac, P. Musienko, Pdms-based stretchable multi-electrode and chemotrode array for epidural and subdural neuronal recording, electrical stimulation and drug delivery n.d., US 10,130,274,B2, **2018**.
[20] D. N. Hill, S. B. Mehta, D. Kleinfeld, *J. Neurosci.* **2011**, *31*, 8699.
[21] L. Q. Uddin, *Trends in Cognitive Sciences* **2020**, *24*, 734.
[22] C. Boehler, S. Carli, L. Fadiga, T. Stieglitz, M. Asplund, *Nat. Protoc.* **2020**, *15*, 3557.
[23] K. D. Harris, R. Q. Quiroga, J. Freeman, S. L. Smith, *Nat. Neurosci.* **2016**, *19*, 1165.
[24] K. A. Ludwig, J. D. Uram, J. Yang, D. C. Martin, D. R. Kipke, *J. Neural Eng.* **2006**, *3*, 59.
[25] Z. Zhao, R. Gong, L. Zheng, J. Wang, *Sensors* **2016**, *16*, 1851.
[26] J. P. Neto, P. Baião, G. Lopes, J. Frazão, J. Nogueira, E. Fortunato, P. Barquinha, A. R. Kampff, *Front. Neurosci.* **2018**, *12*, 715.
[27] X. Liu, A. Demosthenous, N. Donaldson, *Med. Biol. Eng. Comput.* **2008**, *46*, 997.
[28] V. Parkula, M. S. Maglione, S. Casalini, Q. Zhang, P. Greco, C. A. Bortolotti, C. Rovira, M. Mas-Torrent, F. Biscarini, *Adv Elect Materials* **2019**, *5*, 1800875.
[29] M. Bianchi, A. De Salvo, M. Asplund, S. Carli, M. Di Lauro, A. Schulze-Bonhage, T. Stieglitz, L. Fadiga, F. Biscarini, *Adv. Sci.* **2022**, *9*, 2104701.
[30] D. A. Koutsouras, P. Gkoupidenis, C. Stolz, V. Subramanian, G. G. Malliaras, D. C. Martin, *ChemElectroChem* **2017**, *4*, 2321.
[31] S. Guzzo, S. Carli, B. Pavan, A. Lunghi, M. Murgia, M. Bianchi, *Nanomaterials* **2021**, *11*, 2022.
[32] X. Ren, M. Yang, T. Yang, C. Xu, Y. Ye, X. Wu, X. Zheng, B. Wang, Y. Wan, Z. Luo, *ACS Appl. Mater. Interfaces* **2021**, *13*, 25374.
[33] A. Pisciotta, A. Lunghi, G. Bertani, R. Di Tinco, L. Bertoni, G. Orlandi, F. Biscarini, M. Bianchi, G. Carnevale, *Front. Physiol.* **2022**, *13*, 930804.
[34] J. Rivnay, S. Inal, B. A. Collins, M. Sessolo, E. Stavrinidou, X. Strakosas, C. Tassone, D. M. Delongchamp, G. G. Malliaras, *Nat. Commun.* **2016**, *7*, 11287.
[35] B. D. Paulsen, K. Tybrandt, E. Stavrinidou, J. Rivnay, *Nat. Mater.* **2020**, *19*, 13.
[36] D. T. Simon, E. O. Gabrielsson, K. Tybrandt, M. Berggren, *Chem. Rev.* **2016**, *116*, 13009.
[37] D. C. Martin, G. G. Malliaras, *ChemElectroChem* **2016**, *3*, 686.
[38] M. Di Lauro, A. De Salvo, G. C. Sebastianella, M. Bianchi, S. Carli, M. Murgia, L. Fadiga, F. Biscarini, *ACS Appl. Electron. Mater.* **2020**, *2*, 1849.
[39] S. Venkatraman, J. Hendricks, Z. A. King, A. J. Sereno, S. Richardson-Burns, D. Martin, J. M. Carmena, *IEEE Trans. Neural Syst. Rehabil. Eng.* **2011**, *19*, 307.
[40] N. Kim, S. Kee, S. H. Lee, B. H. Lee, Y. H. Kahng, Y. Jo, B. Kim, K. Lee, *Adv. Mater.* **2014**, *26*, 2268.
[41] C. Xie, Z. Lin, L. Hanson, Y. Cui, B. Cui, *Nature Nanotech* **2012**, *7*, 185.
[42] M. Nikkhah, J. Rivnay, *Acta Biomater.* **2022**, *139*, 1.
[43] G. E. Fenoy, O. Azzaroni, W. Knoll, W. A. Marmisollé, *Chemosensors* **2021**, *9*, 212.
[44] L. Hao, D. Yu, *Synth. Met.* **2022**, *290*, 117138.
[45] Y. Liang, J. C.-H. Goh, *Bioelectricity* **2020**, *2*, 101.
[46] G. C. Sebastianella, M. Di Lauro, M. Murgia, M. Bianchi, S. Carli, M. Zoli, L. Fadiga, F. Biscarini, *Adv Elect Materials* **2021**, *7*, 2100755.
[47] M. Bianchi, S. Guzzo, A. Lunghi, P. Greco, A. Pisciotta, M. Murgia, G. Carnevale, L. Fadiga, F. Biscarini, *ACS Appl. Mater. Interfaces* **2023**, *15*, 59224.
[48] G. Hong, C. M. Lieber, *Nat. Rev. Neurosci.* **2019**, *20*, 330.
[49] J. Yang, D. C. Martin, *Sens. Actuators, B* **2004**, *101*, 133.
[50] Z. Aqrawe, J. Montgomery, J. Travas-Sejdic, D. Svirskis, *Sens. Actuators, B* **2018**, *257*, 753.
[51] M. Du, S. Guan, L. Gao, S. Lv, S. Yang, J. Shi, J. Wang, H. Li, Y. Fang, *Small* **2019**, *15*, 1900582.
[52] A. Lunghi, A. Mariano, M. Bianchi, N. B. Dinger, M. Murgia, E. Rondanina, A. Toma, P. Greco, M. Di Lauro, F. Santoro, L. Fadiga, F. Biscarini, *Adv Materials Inter* **2022**, *9*, 2200709.
[53] F. Santoro, J. Schnitker, G. Panaitov, A. Offenhäusser, *Nano Lett.* **2013**, *13*, 5379.
[54] A. Fendyur, N. Mazurski, J. Shappir, M. E. Spira, *Front. Neuroeng.* **2011**, *4*, https://doi.org/10.3389/fneng.2011.00014.
[55] D. Decker, R. Hempelmann, H. Natter, M. Pirrung, H. Rabe, K. H. Schäfer, M. Saumer, *Adv Materials Technologies* **2019**, *4*, 1800436.
[56] P. Shokoohimehr, B. Cepkenovic, F. Milos, J. Bednár, H. Hassani, V. Maybeck, A. Offenhäusser, *Small* **2022**, *18*, 2200053.
[57] L. Hanson, Z. C. Lin, C. Xie, Y. Cui, B. Cui, *Nano Lett.* **2012**, *12*, 5815.
[58] P. D. Jones, A. Moskalyuk, C. Barthold, K. Gutöhrlein, G. Heusel, B. Schröppel, R. Samba, M. Giugliano, *Front. Neurosci.* **2020**, *14*, 405.
[59] H. Majd, S. S. Scherer, S. Boo, S. Ramondetti, E. Cambridge, W. Raffoul, M. Friedrich, B. Pittet, D. Pioletti, B. Hinz, G. Pietramaggiori, *Biomaterials* **2015**, *54*, 136.
[60] C.-W. Yeh, L.-W. Wang, H.-C. Wu, Y.-K. Hsieh, J. Wang, M.-H. Chen, T.-W. Wang, *Biofabrication* **2017**, *9*, 015024.
[61] Y. Chen, Z. Luo, W. Meng, K. Liu, Q. Chen, Y. Cai, Z. Ding, C. Huang, Z. Zhou, M. Jiang, L. Zhou, *Small* **2024**, *20*, 2310325.
[62] I. Muguet, A. Maziz, F. Mathieu, L. Mazenq, G. Larrieu, *Adv. Mater.* **2023**, *35*, 2302472.
[63] D. Khodagholy, T. Doublet, M. Gurfinkel, P. Quilichini, E. Ismailova, P. Leleux, T. Herve, S. Sanaur, C. Bernard, G. G. Malliaras, *Adv. Mater.* **2011**, *23*, H268.
[64] F. Milos, G. Tullii, F. Gobbo, F. Lodola, F. Galeotti, C. Verpelli, D. Mayer, V. Maybeck, A. Offenhäusser, M. R. Antognazza, *ACS Appl. Mater. Interfaces* **2021**, *13*, 23438.
[65] S. Fan, L. Qi, J. Li, D. Pan, Y. Zhang, R. Li, C. Zhang, D. Wu, P. Lau, Y. Hu, G. Bi, W. Ding, J. Chu, *Adv Healthcare Materials* **2021**, *10*, 2100094.
[66] T. Repić, K. Madirazza, E. Bektur, D. Sapunar, *Sci. Rep.* **2016**, *6*, 39560.
[67] C. Chen, X. Dong, K.-H. Fang, F. Yuan, Y. Hu, M. Xu, Y. Huang, X. Zhang, D. Fang, Y. Liu, *Acta Pharm. Sin. B* **2019**, *9*, 557.
[68] Y. Liu, A. F. McGuire, H.-Y. Lou, T. L. Li, J. B.-H. Tok, B. Cui, Z. Bao, *Proc. Natl. Acad. Sci. U.S.A.* **2018**, *115*, 11718.
[69] T. Marciuš, A.-F. Deftu, I. Vuka, D. Braeken, D. Sapunar, *J. Neurosci. Methods* **2024**, *407*, 110143.
[70] S. Shukla, J. L. Schwartz, C. Walsh, W. M. Wong, V. Patel, Y.-P. Hsieh, C. Onwuasoanya, S. Chen, A. Offenhäusser, G. Cauwenberghs, F. Santoro, A. R. Muotri, G. W. Yeo, S. H. Chalasani, Z. Jahed, *Microsyst. Nanoeng.* **2024**, *10*, 184.
[71] M. Bianchi, S. Carli, M. Di Lauro, M. Prato, M. Murgia, L. Fadiga, F. Biscarini, *J. Mater. Chem. C* **2020**, *8*, 11252.
[72] J. Rivnay, M. Ramuz, P. Leleux, A. Hama, M. Huerta, R. M. Owens, *Appl. Phys. Lett.* **2015**, *106*, 043301.
[73] E. Kublic, *Acta Neurobiologiae experimentals* **2004**, *64*, 229.
[74] Y. Xia, G. M. Whitesides, *Annu. Rev. Mater. Sci.* **1998**, *28*, 153.
[75] S. M. Rossnagel, *IBM J. Res. & Dev.* **1999**, *43*, 163.
[76] D. Qi, K. Zhang, G. Tian, B. Jiang, Y. Huang, *Adv. Mater.* **2021**, *33*, 2003155.
[77] M. ElMahmoudy, S. Inal, A. Charrier, I. Uguz, G. G. Malliaras, S. Sanaur, *Macro Materials & Eng* **2017**, *302*, 1600497.
[78] F. Decataldo, T. Cramer, D. Martelli, I. Gualandi, W. S. Korim, S. T. Yao, M. Tessarolo, M. Murgia, E. Scavetta, R. Amici, B. Fraboni, *Sci. Rep.* **2019**, *9*, 10598.
[79] C. Py, P. Reverdy, L. Doppler, J. Bico, B. Roman, C. N. Baroud, *Phys. Rev. Lett.* **2007**, *98*, 156103.

[80] C. Py, P. Reverdy, L. Doppler, J. Bico, B. Roman, C. N. Baroud, *Eur. Phys. J. Spec. Top.* **2009**, *166*, 67.
[81] I. Rembado, E. Castagnola, L. Turella, T. Ius, R. Budai, A. Ansaldo, G. N. Angotzi, F. Debertoldi, D. Ricci, M. Skrap, L. Fadiga, *Int. J. Neur. Syst.* **2017**, *27*, 1650052.
[82] G. Buzsáki, *Rhythms of the Brain*, Oxford Univeristy Press, Oxford, England **2006**.
[83] S. Di, D. S. Barth, *Brain Res.* **1991**, *546*, 106.
[84] J. Viventi, D.-H. Kim, L. Vigeland, E. S. Frechette, J. A. Blanco, Y.-S. Kim, A. E. Avrin, V. R. Tiruvadi, S.-W. Hwang, A. C. Vanleer, D. F. Wulsin, K. Davis, C. E. Gelber, L. Palmer, J. Van Der Spiegel, J. Wu, J. Xiao, Y. Huang, D. Contreras, J. A. Rogers, B. Litt, *Nat. Neurosci.* **2011**, *14*, 1599.
[85] A. Suarez-Perez, G. Gabriel, B. Rebollo, X. Illa, A. Guimerà-Brunet, J. Hernández-Ferrer, M. T. Martínez, R. Villa, M. V. Sanchez-Vives, *Front. Neurosci.* **2018**, *12*, 862.